PROCEEDINGS of the
23rd International Congress on Acoustics

9 to 13 September 2019 in Aachen, Germany

Acquisition of Bi-Directional Reflectance Functions by Nearfield Acoustical Holography – a preliminary study

Jonathan Andrew HARGREAVES[1]

[1] University of Salford, United Kingdom

ABSTRACT

It is well known that material absorption and scattering is dependent on incidence and observation angle. Despite this, the corresponding standardised coefficients, which are used to represent these mechanisms within computational acoustic models, aggregate all such dependency into single random-incidence parameters. This limits the accuracy that can be achieved with computational acoustic models – even if these algorithms were to capture the wave physics perfectly, which they often do not, the results would not match physical reality because the input data is too low resolution. Bi-Directional Reflectance Functions are an established way of describing boundary absorption and scattering in computer graphics that have been suggested for use in acoustics. To date, several algorithms have been published that do or could use these in simulation, but no measurement methods are available to acquire them. There is also ambiguity over some aspects of their definition e.g. whether finite panel size is included as a scattering mechanism. This paper adopts a definition suitable for high-frequency Boundary Element Method algorithms that use oscillatory basis functions to capture wave directions. It then proposes an acquisition method based on double-layer Near-Field Acoustical Holography and assesses it accuracy using 2D simulations.

Keywords: Room Acoustics, Microphone Array Methods, Scattering

1. INTRODUCTION AND BACKGROUND

Methods to measure the acoustic absorption of materials have long been of interest and various approaches are standardised e.g. ISO 354:2003 (random-incidence in a reverberation room), ISO 10534-2:2001 (normal-incidence in an impedance tube) or ISO 13472-1:2002 (free-field). Accurate material absorption data is known to be a prerequisite if computational room acoustic models are required to be accurate (1–3). This is particular clear when algorithms such as Boundary Element Method (BEM) are applied; these are capable of producing extremely accurate results if the material data is precisely known, but will still produce inaccurate results when it is not (4). ISO 10534-2:2001 is presently the most accurate standardised technique for absorption measurement, and can capture surface impedance as well as absorption coefficient, but applying it for existing spaces is destructive (5). There has therefore been a recent surge in interest in 'in-situ' methods (6) and, of these, Nearfield Acoustical Holography (NAH) techniques show particular promise. For example the recent method by Hald et al (7) can be applied in an untreated room and requires only compact samples and hardware. It is also capable of measuring the angle-dependence of the absorption of homogeneous samples.

Scattering from boundaries or obstacles is also known to be an important mechanism within Room Acoustics, with specialist 'diffusers' often being installed to subjectively improve the acoustics for music performance or critical listening spaces (8). Its inclusion in room acoustic modelling software has also been shown to be necessary to achieve realistic results (1), and predicted values for room acoustic metrics depend strongly on the strength and type of scattering mechanism chosen (2). It is therefore now included in all commercial room acoustic modelling software, usually following the random-incidence scattering coefficient that is measured according to ISO 17497-1:2004. The current situation remains far from ideal though; there is relatively little measured scattering data available and what does exist typically has high uncertainty attached to it, leaving practitioners to make 'best guesses' based on what seems to have worked satisfactorily in the past. There is also the issue that no detail is captured about the nature of the scattering; devices that redirect sound or that scatter in only one plane, such as the extruded diffusers common in concert halls, are not well characterised.

[1] j.a.hargreaves@salford.ac.uk

1.1 Directional Scattering Measurement

It is perhaps no surprise therefore that the group who have previously been most interested in measuring higher-resolution angle-dependent scattering data are diffuser designers. D'Antonio discussed the possibility of standardising this as early as 1992 (9), but a scalar 'diffusion coefficient' to quantity uniformity of scattering was ultimately standardised in ISO 17497-2:2012 instead; this also includes an alternative scattering coefficient definition. The standard does however include detail on how to measure high-resolution angle-dependent scattering because that is the raw data from which the coefficients are extracted. This is achieved using a so-called 'goniometer' setup, where both the source and sensors are in the quasi-far field of the object to be measured.

There are several problems with this approach in the author's opinion. Firstly, there are issues of practicality. They rely on subtraction approaches to separate incident and scattered sound, so require very low background noise, time invariant conditions (e.g. temperature), and either an anechoic environment or a very large room with time-gating to eliminate contamination from other reflections. The rigs are also large and unwieldly to apply in situ (10). Secondly, their design is fundamentally incompatible with the way that the directional data they measure could be used in Geometrical Acoustics (GA) simulation algorithms. These assume an unrealistic model of acoustic wave propagation as geometric rays or beams, the reflection of which from a boundary is most closely approximated by far-field (i.e. plane wave) excitation and measurement with an infinite-sized sample. The latter restriction occurs because GA models reflection and scattering as a local phenomenon; the edge effects that occur in measurement due to finite sample size should not factor and require removal from the dataset. We therefore distinguish between local scattering, that could occur to surface undulations and roughness, and the leading-order edge diffraction that occurs at the edges of panels. The preferred approach is that the latter should be handled separately in the simulation algorithm (11), hence the task of measuring panel scattering is to quantify only the former. This is a useful distinction but one that has been muddied by the common practice of adjusting scattering coefficient to mask the worst errors occurring due to absence of diffraction in GA simulation algorithms (12).

Goniometers are, by nature of their design, restricted to finite sample size and measurement and excitation distances. The requirement from GA for far-field measurements of infinite-sized samples are both contradictory and unachievable with the goniometer 'one physical source / sensor per measurement / observation angle' paradigm. The coefficients defined in ISO 17497-2:2012 include normalisation for finite sample size, but this is not the same as correcting the raw directional measured data. Measurements of directional reflection and/or scattering with phase, as would be ideal for early reflections that provide critical spatial cues, is certainly out of the question.

1.2 Scattering Measurement by Nearfield Acoustical Holography

The issue of finite sample size is circumvented by measuring in the nearfield; edge effects are relatively less significant due to proximity to the sample and can be corrected for if required (13). Far-field data can also be recovered mathematically by applying the far-field approximation to the Kirchhoff-Helmholtz boundary integral equation (14), often termed "nearfield to far-field transform". Usually this utilises a plane-wave decomposition, though Müller-Trapet (15) investigated representing scattering using spherical harmonic functions; there it was assumed that this means the microphone array also has to be spherical, though work by this author shows that this is not the case (16,17).

D'Antonio (9) was aware of the usefulness of NAH in 1992 through its pioneering application to surface impedance measurement by Tamura (18,19) in 1990, but appears to have concluded that it required sample isotropy; that was true for the method of Tamura, which assumed specular reflection, but is not a limitation of NAH in general. Kleiner et al (20) actually used NAH to measure directional scattering in 1995, though here were attempting to include finite sample size effects to as to mimic the results acquired by goniometers, and viewed the difficulty in doing this as a limitation rather than an advantage. Such early studies were limited by the availability and cost of multi-channel acquisition hardware, which today is ubiquitous. Separation of incident and reflected waves was also an issue, with researchers often resorting to subtraction techniques. Today, multichannel integrated double-layer pressure-sensing (PP) microphone arrays are available, as are integrated pressure and particle-velocity (PU) sensors, that enable this issue to be overcome.

1.3 Representation of Scattering in Acoustic Simulation Algorithms

Commercial room acoustic simulation algorithms are almost exclusively GA based, and that paradigm will be assumed here. We therefore wish to represent how an incoming wave with amplitude

A_i arriving from an incident angle $(\theta_\mathrm{i}, \phi_\mathrm{i})$ might give rise to a distribution of outgoing waves with amplitudes $A_\mathrm{o}(\theta_\mathrm{o}, \phi_\mathrm{o})$; here θ is azimuth and ϕ is polar angle. The function R that relates these must be a function of both pairs of angles, hence $R(\theta_\mathrm{o}, \phi_\mathrm{o}, \theta_\mathrm{i}, \phi_\mathrm{i})$. Siltanen et al (21) refer to this a Bi-Directional Reflectance Function (BDRF), a term transferred from computer graphics. It can also predict the amplitude at a given outgoing angle, given the incoming distribution $A_\mathrm{i}(\theta_\mathrm{i}, \phi_\mathrm{i})$, by $A_\mathrm{o}(\theta_\mathrm{o}, \phi_\mathrm{o}) = R(\theta_\mathrm{o}, \phi_\mathrm{o}, \theta_\mathrm{i}, \phi_\mathrm{i}) \otimes A_\mathrm{i}(\theta_\mathrm{i}, \phi_\mathrm{i})$; here $\otimes$ represents a two-dimensional convolution over θ_i and ϕ_i. The BDRF is about the most general representation of geometric scattering one could have, especially if it is also deemed to be position dependent, and Siltanen et al argued how it encompasses previous approaches and showed how it can be applied to a variety of GA algorithms.

BDRFs do however have limitations when applied to acoustics. When used with raytracing in computer graphics, it is reasonable for a BDRF to vary spatially in an arbitrary way; this is because light's very short wavelength means optical scattering structures are orders of magnitude smaller than the geometry being modelled. For acoustics in contrast, wavelength is comparable to the size of geometric features in many cases, meaning angular and spatial variation of BDRFs are inextricably interlinked. Subject to these restrictions, BDRFs can best be understood as representing acoustic scattering in some spatially averaged sense that uses a particular choice of spatial window function defined on the boundary. Understanding the effect of this for both measurement and simulation requires consideration beyond the GA paradigm, and some initial analysis will be presented herein. In particular, the transition from diffraction due to panel size to scattering due to surface roughness is essentially a 'mid-frequency' problem, so techniques developed for high-frequency BEM (22) can be useful. These algorithms interpolate pressure fields using oscillatory basis functions that are designed to capture leading-order propagation directions (23), which may even be found using a geometric method (24). The radiation from these basis functions rather resembles geometric beams as frequency increases; some can be stated as a geometric beam plus a correction term (25). One recent algorithm (26), like GA, uses reflectance boundary conditions and is solved by marching on in reflection order.

Following the acknowledgement that acoustic BDRFs must be understood in a spatially-averaged sense over some surface 'patch', the category of algorithms to which they are most suited is what Svensson and Savioja (27) class as "surface-based" GA. Those that discretise wave arrival and reflection angles, in addition to spatial discretization with a mesh, have been given various names including 'Acoustic Radiance Transfer' (ART) (21) and 'Dynamical Energy Analysis' (DEA) (28). BDRFs will also require discretisation over space and angle; notably, if this matches what is used in the simulation algorithm then the convolution above becomes a straightforward matrix multiplication. Siltanen et al proposed piecewise-constant angular discretisation, but Chappell and co-workers developed superior hierarchical schemes based on Legendre polynomials in 2D (28) and Zernike polynomials in 3D (29). Both groups used discontinuous spatial discretisation, however continuous spatial discretisation will be employed here because it produces beams that are more geometric in nature (25), aids convergence of high-frequency BEM (26) and reduces microphone array sidelobes.

2. MODELLING FRAMEWORK AND TESTBED

When using BDRFs in a numerical model, the primary objective is to replace a complicated boundary Γ, which is either costly to simulated or can only be measured, with a simplified boundary Γ_s with BDRFs that give equivalent scattering behaviour and absorption. A numerical testbed is useful since reflections computed from BDRFs on the simplified boundary can be validated against reflections computed using a direct model of the complicated boundary e.g. using BEM.

Figure 1a show the configuration. A sample with complicated boundary Γ (black) lies below a fictional simplified boundary Γ_s (dashed blue); this is shown as being planar but needn't necessarily be due to the findings in (16) and (26). An incoming plane wave (green) excites the sample causing an outgoing wave (purple) to be scattered. Both are sensed by a microphone array (blue dots) located on Γ_s. This arrangement of having the output data (BDRFs) defined on the same surface that is for measurement is unusual for NAH; it is more common to back-propagate the measured data to the physical boundary that

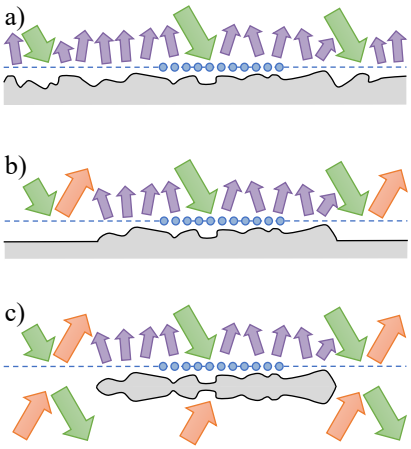

Figure 1 Procedure to produce a local model for BDRF evaluation.

produced it e.g. so that boundary vibration can be found. This step is unnecessary for the intended application, however, and is usually ill-posed so avoiding it is advantageous.

The Kirchhoff-Helmholtz boundary integral equation, being the mathematical foundation of BEM, is useful for analysing this problem. It says that if pressure and particle velocity are known on the entire simplified boundary, then the reflections from the complicated boundary can be perfectly reproduced from that data. This is a useful benchmark but is impractical for entire scenarios since generating this data requires solution with an accurate algorithm such as BEM over the entire complicated boundary. If this can be done reasonable effort then it renders the entire encoding as BDRFs process pointless.

Instead it is desirable to exploit the assumption that scattering is a local phenomenon and try and acquire BDRFs via local simulations that are much computationally cheaper. There is precedent for this in diffusion coefficient measurement and simulation; no one expects to have to simulate an entire concert hall to understand how a diffuser performs, and BEM simulations of small samples have been shown to be very effective (8). The complicated boundary could of course be simply truncated but this would likely produce strong edge effects, hence Figure 1b&c propose a more sophisticated approach. In Figure 1b the complicated boundary is truncated but embedded in an infinite planar baffle; this reduces truncation effects but means that the reflected wave (orange) from these sections can be computed analytically. To avoid meshing the planar baffle, symmetry is exploited in Figure 1c, reflecting both the obstacle and the incident wave, which then becomes the analytical reflected wave (orange). This approach is widely exploited in BEM and means that only the truncated section of the complicated boundary needs to be meshed, yielding much-reduced computational cost.

2.1 Mathematical Formulation

The mathematical formulation used for the testbed will now be presented. The model is formulated in two dimensions for simplicity; all quantities and geometry are assumed to be invariant of the other third dimension. All quantities are time harmonic with time dependence $\mathrm{e}^{-\mathrm{i}\omega t}$, where ω is frequency expressed in radians per second. Acoustic waves in the air domain have pressure p that satisfies Helmholtz' equation $\nabla^2 p(\mathbf{x}) + k^2 p(\mathbf{x}) = 0$. Here $\mathbf{x}$ is a point in 2D Cartesian space and $k = \omega/c_0$ is the wavenumber, where c_0 is the speed of sound in air. The simplified boundary Γ_s is assumed to be planar for ease of analysis; $\hat{\mathbf{t}}$ and $\hat{\mathbf{n}}$ are respectively its tangential and normal unit vectors and $\hat{\mathbf{n}}$ is deemed to point away from the sample being characterised into the air volume. It is offset a distance d from the coordinate origin, which is taken to align with the sample, hence $\hat{\mathbf{n}} \cdot \mathbf{x} = d$ for all $\mathbf{x} \in \Gamma_\mathrm{s}$.

A key concept in this formulation is that total pressure p_t can be decomposed into an incoming wave with pressure p_i and an outgoing wave with pressure p_o, so $p_\mathrm{t}(\mathbf{x}) = p_\mathrm{i}(\mathbf{x}) + p_\mathrm{o}(\mathbf{x})$. The word "outgoing" has been used here because the more common words "reflected" and "scattered" have been reserved for more specific behaviours. Incidence and reflected wave directions (green and orange in Figure 1) will be parameterised by k_t; the component of wavenumber tangential to the measurement plane. This definition is chosen over one based on angle because it supports inhomogeneous (evanescent) plane waves, for which $|k_\mathrm{t}| > k$. In the non-evanescent region $|k_\mathrm{t}| \leq k$, polar angle ϕ can be found by $\phi = \sin^{-1}(k_\mathrm{t}/k)$. The incoming and outgoing waves have complex amplitude densities $A_\mathrm{i}(k_\mathrm{t})$ and $A_\mathrm{o}(k_\mathrm{t})$ respectively. The pressures p_i and p_o can be found from these by:

$$p_{\mathrm{i|o}}(\mathbf{x}) = \frac{1}{2\pi} \int_{-\infty}^{\infty} A_{\mathrm{i|o}}(k_\mathrm{t}) \mathrm{e}^{\mathrm{i}[k_\mathrm{t}\hat{\mathbf{t}} \mp k_\mathrm{n}\hat{\mathbf{n}}]\cdot\mathbf{x}} dk_\mathrm{t}. \tag{1}$$

The term $\mp$ in the exponent is negative for the incoming wave and positive for the outgoing wave and $k_\mathrm{n} = \sqrt{k^2 - k_\mathrm{t}^2}$ is the component of wavenumber normal to Γ_s. The positive imaginary branch of the square root is chosen when $|k_\mathrm{t}| > k$ because this means the outgoing evanescent waves decay in the direction $\hat{\mathbf{n}}$, which is consistent with the notion that they arise from the sample below. It may be noticed that eq. (1) takes the form of a spatial Fourier transform. Williams (30) calls this system of parameterising wave direction a 'wavenumber spectrum' and it is the basis of classical NAH.

3. Spatial Windowing and BDRFs

A system of spatial discretisation will now be defined. For the reasons mentioned in section 1.3, it is chosen to implement this using smooth spatial windowing functions. The intention is that this scheme could also be used as an approximation space for the reflection-based high-frequency BEM scheme in (26). This means the window functions must form a partition-of-unity, i.e. sum to one.

A system of overlapping raised Hanning windows fulfils these criteria. These have been shown to give improved accuracy compared to non-smooth alternatives in high-frequency BEM (31) and a technique to accelerate evaluation of integrals involving them was presented in (25). They are defined:

$$w(\mathbf{x}) = \left[{}^1\!/_2 + {}^1\!/_2 \cos\left(2\pi\mu(\mathbf{x})\right)\right] \times \Pi\left(\mu(\mathbf{x})\right), \text{ where } \Pi(\mu) = \begin{cases} 1 & |\mu| < {}^1\!/_2 \\ 0 & |\mu| > {}^1\!/_2 \end{cases} \quad (2)$$

Here μ is a normalised local coordinate that runs $-{}^1\!/_2 \leq \mu \leq {}^1\!/_2$ over the support of the window. The windows are length L and are centered on vertices $\mathbf{v}_n = {}^1\!/_2 nL\hat{\mathbf{t}} + d\hat{\mathbf{n}}$, where n is an integer window index, and $\mu(\mathbf{x}) = \hat{\mathbf{t}} \cdot [\mathbf{x} - \mathbf{v}_n]/L$. For each window complex amplitude densities $C_{\mathrm{i},n}(k_\mathrm{t})$ and $C_{\mathrm{o},n}(k_\mathrm{t})$ are defined, allowing p_i and p_o to be found for $\mathbf{x} \in \Gamma_\mathrm{s}$:

$$p_{\mathrm{i|o}}(\mathbf{x}) = \frac{1}{2\pi} \sum_n \int_{-\infty}^{\infty} C_{\mathrm{i|o},n}(k_\mathrm{t}) b(\mathbf{x}, k_\mathrm{t}) dk_\mathrm{t}, \text{ where } b(\mathbf{x}, k_\mathrm{t}) = w(\mathbf{x}) \mathrm{e}^{\mathrm{i}[k_\mathrm{t}\hat{\mathbf{t}} \mp k_\mathrm{n}\hat{\mathbf{n}}] \cdot [\mathbf{x} - \mathbf{v}_n]}. \quad (3)$$

As with eq. (1), the term $\mp$ is negative for the incoming wave and positive for outgoing. Comparing eq. (3) and (1), and noting that the windows form a partition-of-unity, it is apparent that the 'correct' values are $C_{\mathrm{i|o},n}(k_\mathrm{t}) = A_{\mathrm{i|o}}(k_\mathrm{t}) \mathrm{e}^{\mathrm{i}[k_\mathrm{t}\hat{\mathbf{t}} \mp k_\mathrm{n}\hat{\mathbf{n}}] \cdot \mathbf{v}_n} = A_{\mathrm{i|o}}(k_\mathrm{t}) \mathrm{e}^{\mathrm{i}[k_\mathrm{t} Ln/2 \mp k_\mathrm{n} d]}$. Allowing each patch to have its own distribution is however more flexible and can result in individual $C_{\mathrm{i|o},n}$ being sparser than $A_{\mathrm{i|o}}$. To understand this, imagine a spherical wave impinging on a planar surface. $A_{\mathrm{i|o}}$ must capture the curvature of the entire wavefront, so will contain significant amplitude over a wide range of k_t. $C_{\mathrm{i|o},n}$ on the other hand, need only represent a small section of the wavefront which, being quasi planar if the source is some distance away, will result in significant amplitude over a fairly narrow range of k_t.

In a GA algorithm, $C_{\mathrm{i},n}(k_\mathrm{t})$ would be the angular distribution of rays or beams arriving at the n^{th} surface patch, and $C_{\mathrm{o},n}(k_\mathrm{t})$ would be what leaves in response. It follows that the BDRF for the n^{th} surface patch, $R_n(k_{\mathrm{t,o}}, k_{\mathrm{t,i}})$, must relate these so, with $\otimes$ representing convolution over $k_{\mathrm{t,i}}$:

$$C_{\mathrm{o},n}(k_{\mathrm{t,o}}) = R_n(k_{\mathrm{t,o}}, k_{\mathrm{t,i}}) \otimes C_{\mathrm{i},n}(k_{\mathrm{t,i}}). \quad (4)$$

This is our mathematically formalised definition of a patch based BDRF. It has been defined for complex pressure amplitudes but could readily be applied to energy, as proposed in (21), by applying it to squared pressure amplitudes. If $C_{\mathrm{i},n}(k_\mathrm{t})$ and $C_{\mathrm{o},n}(k_\mathrm{t})$ are discretised somehow using a finite set of coefficients in vectors $\mathbf{c}_{\mathrm{i},n}$ and $\mathbf{c}_{\mathrm{o},n}$, then it can be written in matrix form as $\mathbf{c}_{\mathrm{o},n} = \mathbf{R}_n \mathbf{c}_{\mathrm{i},n}$.

4. Measurement of BDRFs

The task of the microphone array is to capture instances of $C_{\mathrm{i},n}(k_\mathrm{t})$ and $C_{\mathrm{o},n}(k_\mathrm{t})$ such that, given sufficient different incident wave conditions, $R_n(k_{\mathrm{t,o}}, k_{\mathrm{t,i}})$ may be derived. It is important however to realise that the array does not measure these directly. Adopting the lexicon of variational BEM (32), $C_{\mathrm{i},n}$ and $C_{\mathrm{o},n}$ are termed 'Coefficients'; their values correctly represent p_i and p_o. The distributions that the array will measure are termed 'Projections'. Evaluating these in BEM would typically involve an inner-product integral along the measurement surface; a simple windowed beamformer would be:

$$P_{\mathrm{i|o},n}(k_\mathrm{t}) = \int_{\Gamma_\mathrm{s}} p_{\mathrm{i|o}}(\mathbf{x}) b^*(\mathbf{x}, k_\mathrm{t}) dl_\mathbf{x}. \quad (5)$$

This also takes the form of a spatial Fourier transform, but $p_{\mathrm{i|o}}(\mathbf{x})$ has been multiplied by $w(\mathbf{x})$. This becomes convolution in the k_t domain, leading to $P_{\mathrm{i|o},n}(k_\mathrm{t}) = C_{\mathrm{i|o},n}(k_\mathrm{t}) \otimes W(k_\mathrm{t})$, where $W(k_\mathrm{t})$ is the wavenumber spectrum of the window; for the choice of window used herein it is:

$$W(k_\mathrm{t}) = \frac{L}{2} \mathrm{sinc}\left(\frac{k_\mathrm{t} L}{2}\right) + \frac{L}{4} \mathrm{sinc}\left(\frac{k_\mathrm{t} L}{2} + \pi\right) + \frac{L}{4} \mathrm{sinc}\left(\frac{k_\mathrm{t} L}{2} - \pi\right). \quad (6)$$

This convolution with $W(k_\mathrm{t})$ has the effect of spectrally 'smudging' the desired spectrum $C_{\mathrm{i|o},n}(k_\mathrm{t})$ giving the spectrum $P_{\mathrm{i|o},n}(k_\mathrm{t})$ measured by the array. Tamura (18) was aware of this issue but seemed primarily concerned with how it interacted with the high k_t limit due to finite spatial resolution; he mitigated this by using a dipole source that had a more favourable excitation spectrum. Wang-Lin et al (33) studied the performance of Hanning and Tukey windows in this application in 2017, showing that both outperformed the rectangular windowing of Tamura; the spectrum of this is $L \times \mathrm{sinc}(k_\mathrm{t} L/2)$, which decays slower with k_t than the Hanning window spectrum in eq. (6).

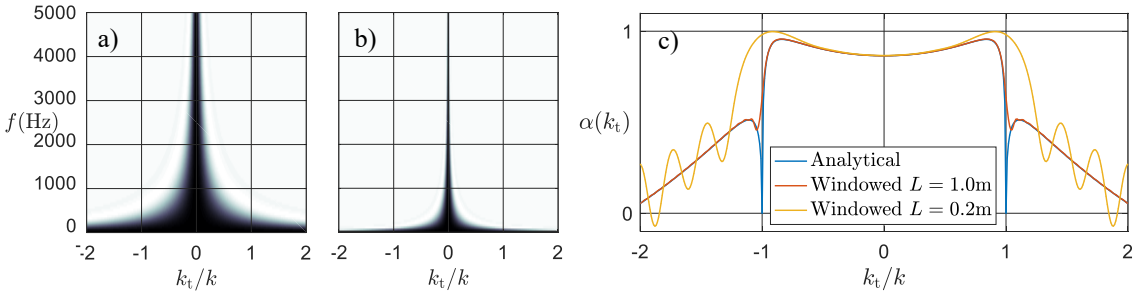

Figure 2: Effect of spatial window. Amplitude of spectral 'smudging' function for a) $L = 0.2$m and b) $L = 1.0$m. c) Effect on absorption coefficient measurement under dipole excitation at 2kHz.

Another reason why these authors did not run into problems is that their measure apertures were very large, being 1.8m diameter in (18) and 2.48m in (33). At these sizes the 'smudging' effect is negligible over the majority of the frequency range of interest. Portable NAH arrays are however much smaller. Hald et al (7) used an array that was only 0.2m across; the amplitude of $W(k_t)$ for $L = 0.2$m is shown in Figure 2a and can be seen to be significant over the full frequency range of interest. In this study a compromise value of $L = 1.0$m has been chosen; $W(k_t)$ for that is shown in Figure 2b.

In terms of measuring BDRFs using projections, spectral 'smudging' would occur for both $C_{i,n}$ and $C_{o,n}$ on the left and right of eq. (4). An approximate BDRF found from $P_{i,n}$ and $P_{o,n}$ would therefore experience both pre-convolution and post-deconvolution with $W(k_t)$ compared to one computed exactly. This actually has zero effect if the incident wave is wavenumber pure and the sample is specularly reflecting, but in all other cases it will cause approximation.

To illustrate this, a uniform and infinite porous material sample has been simulated. The material is 10cm thick, has a flow resitivity of 50,000Nm^{-4}s and is modelled using the approach in (7) to give normalised surface admittacne $Y_s(k_t)$. The sample reflects specularly and the exact BDRF is given by $R_n(k_{t,o}, k_{t,i}) = \delta(k_{t,o} - k_{t,i})\left[k_{n,i}/k - Y_s(k_{t,i})\right]/\left[k_{n,i}/k + Y_s(k_{t,i})\right]$.

In the first test, the incident wave was a single plane wave of unit amplitude and tangential wavenumber $k_{t,inc}$, hence $C_{i,n}(k_{t,i}) = \delta(k_{t,i} - k_{t,inc})$. The outgoing spectrum $C_{o,n}$ was found by convolution of $C_{i,n}$ with R_n, then $P_{i,n}$ and $P_{o,n}$ were found by convolving W with $C_{i,n}$ and $C_{o,n}$ respectively. $k_{t,inc}$ was varied and the BDRF was estimated as $P_{o,n}(k_{t,inc})/P_{i,n}(k_{t,inc})$, which is reasonable since the sample was known to reflect specularly, and this was compared to the exact value. As expected, the BDRF, and the absorption coefficient that can be calculated from it, matched exactly.

In the second test, the sample was subject to excitation from a dipole source and the BDRF for all angles was measured simultaneously on the assumption of specular reflection; this mimics the approach used in (18) and (33). The incoming spectrum was set as $C_{I,n}(k_{t,i}) = e^{ik_n z_0}$, following the trend given in (18) where $z_0 = 1$m is the height of the source above the measurement plane, and the same processing was performed. The results for this are shown in Figure 2c as absorption coefficient extracted from the BDRFs; the exact analytical value is compared to values computed using $L = 0.2$m and $L = 1.0$m. Both array sizes perform well around normal incidence $\equiv k_t = 0$. However, at $k_t = k$ the absorption coefficient varies rapidly as the incident wave transitions into the evanescent region, and at this point the smudging due to the window functions has a noticeable effect; for the smaller array, especially, there is significant oscillation and error. The true reflection coefficient for a finite sample in real life is unlikely to vary as extremely as this – it is a quirk of the mathematical model of infinite plane waves and planar boundaries – but it is true that oblique incident angles are challenging. It is interesting to note that the troublesome 75° measurement in (7) falls at $\sin 75° = 0.96$ on a k_t/k scale, indicating how compressed oblique angles are in k_t and therefore vulnerable to 'smudging'.

5. SEPARATING INCOMING AND OUTGOING WAVES

The above approach required that p_i and p_o were known separately; the projection operator in eq. (5) cannot differentiate between them. This is troublesome in reality since it can only be achieved by subtraction, as applied in (20), which is error-prone and impractical in-situ. A more sophisticated operator that can discriminate between incoming and outgoing waves was defined in (26). It is a generalisation and extension of the array designs of Hulsebos et al (34) and has the physical interpretation of sensing common energy flux between waves (35). For this problem it can be stated as:

$$P_{\mathrm{i|o},n}(k_\mathrm{t}) = \int_{\Gamma_\mathbf{s}} \left[\frac{\partial p_\mathrm{t}}{\partial n}(\mathbf{x}) b^*(\mathbf{x}, k_\mathrm{t}) - p_\mathrm{t}(\mathbf{x}) \frac{\partial b^*}{\partial n}(\mathbf{x}, k_\mathrm{t}) \right] dl_\mathbf{x}. \tag{7}$$

Note that this definition operates on total pressure $p_\mathbf{t}$ rather than p_i or p_o. $\partial/\partial n$ is shorthand for spatial derivative in the direction $\hat{\mathbf{n}}$ i.e. perpendicular to $\Gamma_\mathbf{s}$. $\partial p_\mathrm{t}/\partial n$ may be measured by a particle velocity sensor or a spaced-pair of microphones. $\partial b/\partial n$ can be estimated as $\mp k_\mathrm{n} b$ – note it takes opposite sign for incoming and outgoing waves – but better differentiation between p_i and p_o can be achieved by defining it via a 'Dirichlet to Neumann map' (32); this also takes into account the effect of the window function on the wave. The net result of this is that the measurements of pressure and particle velocity will be windowed differently; particle velocity is multiplied by b^* so is windowed by the original window $w(\mu)$, whereas measured pressure, which is multiplied by $\partial b^*/\partial n$, has a different window $w'(\mu)$ applied to it. Because $w'(\mu)$ is derived from the Dirichlet to Neumann map, it will depend on both k and k_t. Figure 3 shows these for 1kHz with $k_\mathrm{t}/k = {}^1/_2$. While $w(\mu)$ was purely real it turns out the optimal $w'(\mu)$ is complex.

Equation (7) has been applied in a numerical test bed that models an absorbing patch within an infinite rigid baffle using BEM in the configuration depicted in Figure 1; details of and results from this will be included in the conference presentation.

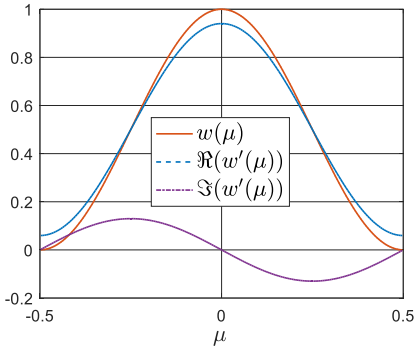

Figure 3: Pressure and particle velocity windows at 1kHz with $L = 1$ and $k_\mathrm{t}/k = {}^1/_2$

6. CONCLUSIONS

This paper has proposed a mathematical formalisation for Bi-Directional Reflectance Functions (BDRFs) for acoustics, including consideration of the effect of the finite patches they must be defined and measured over. It was seen that the common trade-off between spatial windowing and spectral 'smearing' occurs in this application too, and its effect on BDRF measurement was analysed and explored with a numerical test case. Knowledge and formulations from high-frequency variational Boundary Element Method (BEM) have been adopted to assist in the design and analysis. Further work could include attempting to apply other elements of this machinery to mitigate the spectral smudging observed in this study, and to provide a validation approach for partial or whole geometries.

REFERENCES

1. Vorländer M. International Round Robin on Room Acoustical Computer Simulations. In: Newman M, editor. Proceedings of the 15th International Congress on Acoustics. Trondheim; 1995; 689–92.
2. Bork I. A Comparison of Room Simulation Software - The 2nd Round Robin on Room Acoustical Computer Simulation. Acta Acust united with Acust. 2000. 86 (6): 943–56.
3. Vorländer M. Computer simulations in room acoustics: Concepts and uncertainties. J Acoust Soc Am. 2013. 133 (3): 1203–13.
4. Hargreaves JA, Rendell LR, Lam YW. A framework for auralization of boundary element method simulations including source and receiver directivity. J Acoust Soc Am. 2019. 145 (4): 2625–37.
5. Aretz M, Vorländer M. Combined wave and ray based room acoustic simulations of audio systems in car passenger compartments, Part I: Boundary and source data. Appl Acoust. 2014. 76: 82–99.
6. Brandão E, Lenzi A, Paul S. A Review of the *In Situ* Impedance and Sound Absorption Measurement Techniques. Acta Acust united with Acust. 2015. 101 (3): 443–63.
7. Hald J, Song W, Haddad K, Jeong C-H, Richard A. In-situ impedance and absorption coefficient measurements using a double-layer microphone array. Appl Acoust. 2019. 143: 74–83.
8. Cox TJ, D'Antonio P. Acoustic Absorbers and Diffusers: Theory, Design and Application. 2nd ed. Taylor & Francis; 2009. 496 p.
9. D'Antonio P, Konnert J. The Directional Scattering Coefficient: Experimental Determination. J Audio Eng Soc. 1992. 40(12): 997–1017.
10. Ducourneau J, Faiz A, Chatillon J. New device for measuring mapping of sound scattering coefficients of vertical uneven surfaces in a reverberant workplace. Applied Acoustics. 2015. 90: 21-30
11. Svensson UP, Fred RI, Vanderkooy J. An analytic secondary source model of edge diffraction impulse responses. J Acoust Soc Am. 1999. 106 (5): 2331–44.
12. Christensen CL, Rindel JH. A new scattering method that combines roughness and diffraction effects.

In: Forum Acusticum 2005. Budapest, Hungary; 2005;
13. Ottink M, Brunskog J, Jeong C-H, Fernandez-Grande E, Trojgaard P, Tiana-Roig E. In situ measurements of the oblique incidence sound absorption coefficient for finite sized absorbers. J Acoust Soc Am. 2016. 139 (1): 41–52.
14. Richard APA, Fernandez Grande E, Brunskog J, Jeong C-H. Characterization of acoustic scattering from objects via near-field measurements. In: Euronoise 2018. Hersonissos, Crete. p. 2195–202.
15. Müller-Trapet M. Measurement of surface reflection properties : concepts and uncertainties. Phd Thesis. RWTH Aachen; 2015.
16. Hargreaves JA, Lam YW. An Energy Interpretation of the Kirchhoff-Helmholtz Boundary Integral Equation and its Application to Sound Field Synthesis. Acta Acust united with Acust. 2014. 100 (5): 912–20.
17. Hargreaves JA, Lam YW. Corrigendum to An energy interpretation of the Kirchhoff-Helmholtz boundary integral equation and its application to sound field synthesis. Acta Acust united with Acust. 2018. 104 (6): 1134–1134.
18. Tamura M. Spatial Fourier transform method of measuring reflection coefficients at oblique incidence. I: Theory and numerical examples. J Acoust Soc Am. 1990. 88 (5): 2259.
19. Tamura M. Spatial Fourier-transform method for measuring reflection coefficients at oblique incidence. II. Experimental results. J Acoust Soc Am. 1995. 97 (4): 2255–62.
20. Kleiner M, Gustafsson H, Backman J. Measurement of Directional Scattering Coefficients Using Near-Field Acoustic Holography and Spatial Transformation of Sound Fields. In: Audio Engineering Society Convention 99. 1995 Oct;
21. Siltanen S, Lokki T, Kiminki S, Savioja L. The room acoustic rendering equation. J Acoust Soc Am. 2007. 122 (3): 1624.
22. Graham I, Spence E, Chandler-Wilde S, Langdon S. Numerical-asymptotic boundary integral methods in high-frequency scattering. Acta Numer. 2012. 21: 89–305.
23. Hargreaves JA, Lam YW, Langdon S, Hewett DP. A high-frequency BEM for 3D acoustic scattering. In: 22nd International Congress on Sound and Vibration, ICSV 2015. 2015;
24. Groth SP, Hewett DP, Langdon S. A hybrid numerical–asymptotic boundary element method for high frequency scattering by penetrable convex polygons. Wave Motion. 2018. 78: 32–53.
25. Hargreaves JA, Lam YW, Langdon S. A transformation approach for efficient evaluation of oscillatory surface integrals arising in three-dimensional boundary element methods. Int J Numer Methods Eng. 2016. 108 (2): 93–115.
26. Hargreaves JA, Lam YW. The Wave-Matching Boundary Integral Equation — An energy approach to Galerkin BEM for acoustic wave propagation problems. Wave Motion. 2018. 87: 4–36.
27. Savioja L, Svensson UP. Overview of geometrical room acoustic modeling techniques. J Acoust Soc Am. 2015. 138 (2): 708–30.
28. Chappell DJ, Tanner G, Giani S. Boundary element dynamical energy analysis: A versatile method for solving two or three dimensional wave problems in the high frequency limit. J Comput Phys. 2012. 231 (18): 6181–91.
29. Bajars J, Chappell DJ, Søndergaard N, Tanner G. Transport of phase space densities through tetrahedral meshes using discrete flow mapping. J Comput Phys. 2017. 328: 95–108.
30. Williams EG. Fourier acoustics: Sound radiation and nearfield acoustical holography. San Diego: Academic Press; 1999. 306 p.
31. Peake MJ, Trevelyan J, Coates G. Novel basis functions for the partition of unity boundary element method for Helmholtz problems. Int J Numer Methods Eng. 2013. 93 (9): 905–18.
32. Betcke T, van 't Wout E, Gélat P. Computationally Efficient Boundary Element Methods for High-Frequency Helmholtz Problems in Unbounded Domains. In: Modern Solvers for Helmholtz Problems. Birkhäuser; 2017. p. 215–43.
33. Lin W-L, Bi C-X, Opdam R, Zhang Y-B, Vorländer M. Performance of Spatial Windows in the Spatial Fourier Transform Technique for the Angle-Dependent Reflection Factor Measurement. Acta Acust united with Acust. 2017.103 (2): 349–53.
34. Hulsebos E, de Vries D, Bourdillat E. Improved microphone array configurations for auralization of sound fields by Wave Field Synthesis. In: Audio Engineering Society Convention 110. Amsterdam; 2001 May;
35. Hargreaves JA, Lam YW. Acoustic Cross - Energy Measures and Their Applications. In: The 22nd International Congress on Sound and Vibration. Florence; 2015; p. 12–6.